PNAS RESEARCH ARTICLE | MICROBIOLOGY

Trim69 is a microtubule regulator that acts as a pantropic viral inhibitor

Yuxin Song[a], Xuan-Nhi Nguyen[a], Anuj Kumar[a], Claire da Silva[a], Léa Picard[a], Lucie Etienne[a], and Andrea Cimarelli[a,1]

Edited by Michael Oldstone, The Scripps Research Institute, La Jolla, CA; received July 4, 2022; accepted September 20, 2022

Through a screen that combines functional and evolutionary analyses, we identified tripartite motif protein (Trim69), a poorly studied member of the Trim family, as a negative regulator of HIV-1 infection in interferon (IFN)-stimulated myeloid cells. Trim69 inhibits the early phases of infection of HIV-1, but also of HIV-2 and SIV_{MAC} in addition to the negative and positive-strand RNA viruses vesicular stomatitis virus and severe acute respiratory syndrome coronavirus 2, with magnitudes that depend on the combination between cell type and virus. Mechanistically, Trim69 associates directly to microtubules and its antiviral activity is linked to its ability to promote the accumulation of stable microtubules, a program that we uncover to be an integral part of antiviral IFN-I responses in myeloid cells. Overall, our study identifies Trim69 as the antiviral innate defense factor that regulates the properties of microtubules to limit viral spread and highlights the cytoskeleton as an unappreciated battleground in the host-pathogen interactions that underlie viral infections.

virus | interferon | innate response | HIV | SARS-CoV2

Significance

The identification and characterization of proteins capable of inhibiting a large spectrum of viruses is a key objective for our comprehension of the infection process and for the development of broad-spectrum antivirals. Searching for interferon-regulated modulators of HIV-1 infection, we identified tripartite motif protein (Trim69) as a protein endowed with broad antiviral properties. Trim69 acts against HIV-1, primate lentiviruses and the negative- and positive-strand RNA viruses vesicular stomatitis virus and severe acute respiratory syndrome coronavirus 2 by commandeering a general program of microtubule stabilization that is commonly observed in interferon-stimulated myeloid cells and that is detrimental to infection. In a panorama in which several viruses use the cytoskeleton for their own advantage, our study identifies Trim69 as a major innate defense factor that remodels microtubules to limit viral spread.

In recent years, the search for cellular effectors directed against the HIV-1 retrovirus has drawn particular interest, spurring a number of genetic screens that are defining the complex cellular landscape in which HIV replication occurs. In a search for novel interferon-stimulated genes (ISGs) that could interfere with HIV-1 infection, we have examined the weight of more than 400 ISGs during HIV-1 infection of interferon (IFN)-stimulated macrophage-like cells (THP-1-PMA differentiated) that represent a cellular context particularly restrictive to infection (1). Using a three-layer screen approach that combines functional and evolutionary analyses, we have identified the tripartite motif protein (Trim69) as a regulator of the early phases of the life cycle of HIV-1. Trim69 is a poorly studied member of the large Trim family that includes more than 80 members largely devoted to innate immunity regulation (2). In the past, Trim69 had been controversially linked to apoptosis and p53 signaling (3–6), but evidence of strong positive selection suggested this protein could be potentially involved in a host-pathogen genetic conflict (7). Evidence that this could be the case came only in 2018, when Trim69 was reported to inhibit Dengue virus replication through the degradation of the viral nonstructural protein 3 (NS3) (8). While this finding could not be confirmed by a subsequent study (9), two studies identified Trim69 as an inhibitor of the vesicular stomatitis virus (VSV) (9, 10). The underlying mechanism of viral inhibition and more importantly the spectrum of viruses that can be targeted by this protein remain unclear.

In this study, we determine that in myeloid cells, Trim69 is capable of inhibiting not only HIV-1, but also other primate lentiviruses, in addition to the negative-strand RNA virus VSV, and to the positive-strand RNA coronavirus, severe acute respiratory syndrome coronavirus 2 (SARS-CoV-2). These viruses are inhibited to varying degrees depending on the combination between virus and cell type, but overall, our results indicate that Trim69 is an antiviral factor endowed with a broad spectrum of inhibition. Trim69 inhibits the early phases of the above-mentioned viruses at entry and early post-entry phases and, in particular, reverse transcription, entry-primary transcription, and RNA replication for HIV-1, VSV, and SARS-CoV-2, respectively. Antiviral inhibition is linked to the ability of Trim69 to induce the accumulation of stable microtubules, and property that we described here is a previously unrecognized common cellular response to IFN stimulation and distinct from the microtubule (MT) stabilization induced by Taxol. Overall, our results uncover Trim69 as a key modulator of MT dynamics during viral infection and further stress the importance that the control of the cytoskeleton network plays during the host-pathogen conflicts that underlie viral infection.

Author contributions: Y.S. and A.C. designed research; Y.S., X.-N.N., A.K., C.d.S., L.P., and L.E. performed research; L.P. and L.E. contributed new reagents/analytic tools; Y.S., X.-N.N., L.E., and A.C. analyzed data; and A.C. wrote the paper.

The authors declare no competing interest.

This article is a PNAS Direct Submission.

[1]To whom correspondence may be addressed. Email: acimarel@ens-lyon.fr.

This article contains supporting information online at http://www.pnas.org/lookup/suppl/doi:10.1073/pnas.2211467119/-/DCSupplemental.

Published October 17, 2022.

Results

A Three-Layer Genetic Screen to Identify Novel Mediators of the Negative Effects of IFN-I during the Early Phases of HIV-1 Infection in Macrophage-Like Cells. The early phases of HIV-1 infection are inhibited by type 1 interferons and more potently so in cells of the myeloid lineage (1). To identify novel effectors of this antiviral response, we individually silenced >400 ISGs described in the Interferome database by lentiviral-mediated short hairpin RNA (shRNA) transduction in THP-1 cells that were split in two then differentiated into a macrophage-like state with phorbol 12-myristate 13-acetate (PMA). We then examined the susceptibility of these cells to HIV-1 in the presence or absence of IFN-α, using single-round of infection competent viruses coding a Firefly Luciferase reporter. IFN-α modulators were defined as silenced genes that modulated the no IFN-α/IFN-α infectivity ratio (referred to here as the IFN defect) when normalized to the library average value (scheme of Fig. 1*A*).

To exclude modulators of IFN-α signaling rather than of HIV-1 infection per se, a secondary screen was carried out on primary IFN-α hits, by measuring the effects of gene silencing on the production of IP10, a well-described ISG, in THP-1-PMA cells stimulated with IFN-α. A tertiary evolutionary analysis was then performed on remaining hits to prioritize them according to their evolutionary history and their potential roles in host-pathogen evolutionary genetic conflicts, using the DGINN pipeline (detection of genetic innovation) (11).

Under these conditions, the primary functional screen yielded 22 genes with significant impact on HIV-1 infection in the presence of IFN-α (2.5-fold changes, Fig. 1*B* and *SI Appendix*, Fig. S1) for individual values). Given that the IFN defect ratio can also be influenced by the susceptibility to infection of non-stimulated cells (due for instance to different basal levels of expression of the different genes), candidate genes were re-categorized as anti- or pro-viral factors, according to the susceptibility of silenced THP-1-PMA cells during HIV-1 infection in the absence of IFN

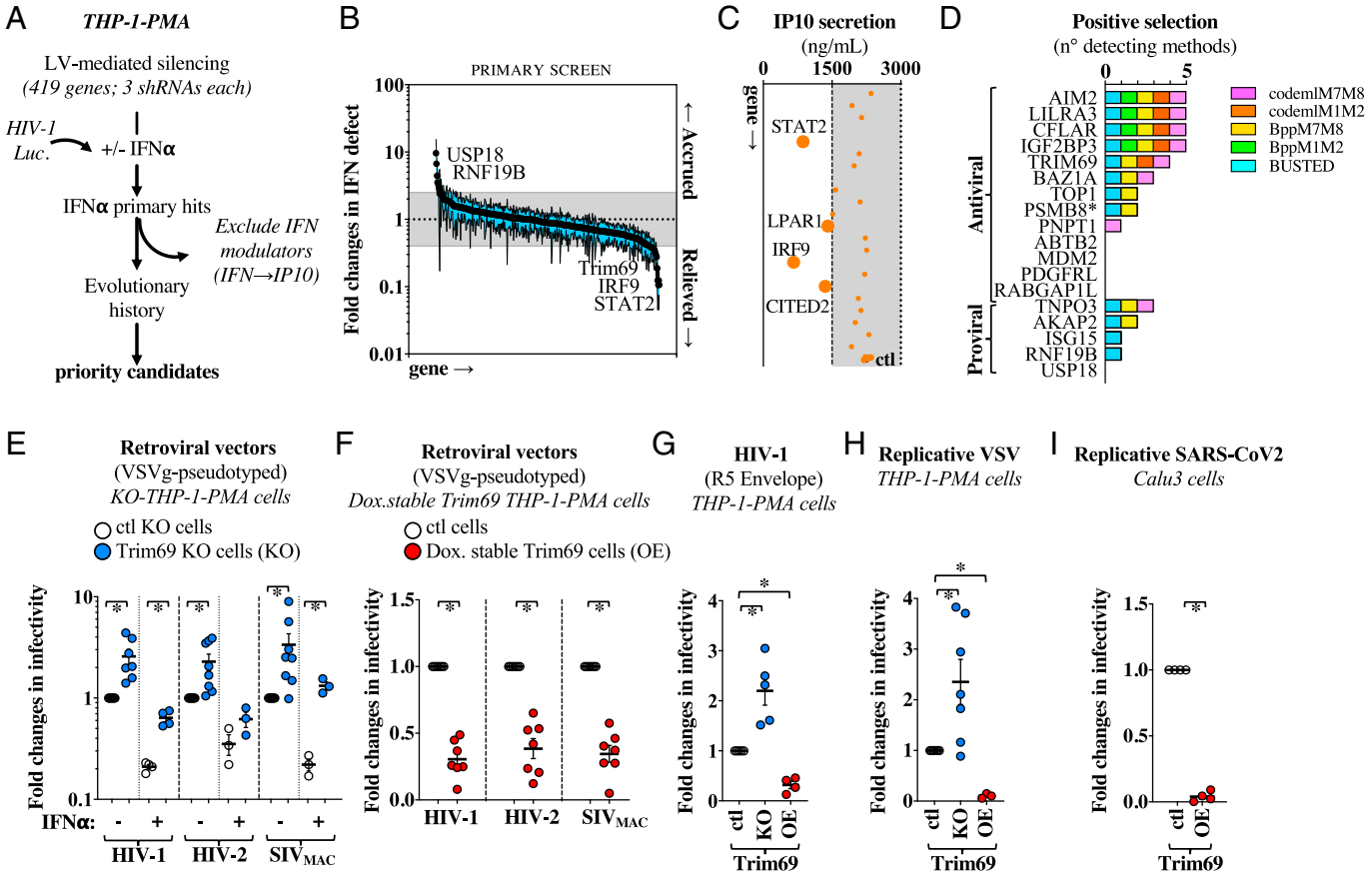

Fig. 1. A three-layer genetic screen for IFN modulators of macrophage infection by HIV-1 highlights Trim69 as a broad viral inhibitor. (*A*) Schematic approach used. ISGs were individually silenced in THP-1 cells by lentiviral-mediated transfer. Cells were then divided in two, differentiated into macrophage-like cells with PMA, treated or not with 1.000 U/mL of IFN-α2 for 24 h prior to viral challenge with a VSVg-pseudotyped HIV-1 virus coding a Firefly luciferase reporter. A secondary screen was carried out on primary hits to exclude genes that interfered with IFN signaling and a tertiary evolutionary screen was carried out on remaining candidates. (*B*) An IFN defect was calculated for each gene (luciferase activities in the no IFN/IFN conditions) and normalized to the average value of the entire library. The graph presents AVG and SEM obtained. A threshold of 2.5 was chosen (outside the gray area) with values >2.5 that indicate accrued IFN defect and values <2.5 that highlight a relieved one. (*C*) Cells silenced for the hits retrieved in (*B*) were stimulated with 1.000 U/mL of IFN-α2 and IP10 was measured by ELISA, 1 d later. Statistically significant differences in IP10 secretion following a one-way ANOVA test. Dunnett's multiple comparison test is represented with larger dots. (*D*) DGINN-mediated positive selection analysis of hits retained after the secondary screen. The graph presents the number of methods that detect positive selection and proteins are separated according to the anti and pro-viral re-categorization provided in the *SI Appendix*, Fig. S1*B*. DGINN also identified a recombination event in PSMB8 and retrieved paralogs for LILRA3 and IGF2BP3 (*SI Appendix*, Fig. S2*C*). (*E*–*G*) THP-1 cells either ablated for Trim69 (KO) or overexpressing (OE) Trim69 under the control of a doxycycline promoter were challenged with the indicated single round of infection viruses coding GFP at multiplicities of infection (MOIs) comprised between 2 and 4. Infection was measured 2–3 d later by fluorescence-activated cell sorter (FACS). (*H* and *I*) Replicative VSV and SARS-CoV-2 viruses bearing a GFP and mNeonGreen reporter, respectively, were used to infect THP-1-PMA cells or epithelial lung Calu-3 cells at MOIs comprised between 0.1 and 0.5. Infection rates were measured either 16 h or 2 d later by FACS. All panels presented AVG and SEM of three to eight independent experiments after normalization. Non-normalized values along with a WB analysis of Trim69 expression levels are presented in the *SI Appendix*, Fig. S5. *Statistically significant differences between the relevant conditions, according to a two-tailed Student's *t* test.

(*SI Appendix*, Fig. S1). Given that silencing of AIM2, TOP1, IGF2BP3, and ABTB2 led to higher HIV-1 infection of unstimulated THP-1-PMA cells, these proteins were re-categorized as antiviral factors. Conversely, silencing of AKAP2 and TNPO3, a well-known HIV cofactor (12) that is not IFN-stimulated but that was introduced in our screen to serve as a sentinel gene, led to lower infection rates in unstimulated cells, so that these proteins were re-categorized as pro-viral factors. The remaining genes did not exhibit significant changes in infectivity in unstimulated cells and were thus not re-categorized. Overall, this analysis led to the identification of five pro- and 17 anti-viral modulators (*SI Appendix*, Fig. S1) that were then analyzed for their ability to interfere with IP10 secretion upon IFN-α stimulation (Fig. 1*C*). Under these conditions, silencing of STAT2, IRF9, as well as of the CBP/p300-interacting transactivator with glutamic acid/aspartic acid-rich carboxyl-terminal domain 2 (CITED2) and the lysophosphatidic acid receptor 1 (LPAR1) significantly decreased IP10 secretion (Fig. 1*C*). While the results obtained with STAT2 and IRF9 were expected, our results highlight a role for CITED2 and LPAR1 in the establishment of an IFN state. For the purpose of this study, the four above-mentioned genes were discarded from subsequent analyses.

Most antiviral restriction factors are engaged into molecular evolutionary arms-races with pathogens (13). They therefore present signatures of these conflicts that can be identified by studying the evolution of their orthologs in host sequences. To identify the candidate genes that present such genetic innovations during primate evolution, we screened the functionally retrieved hits with the DGINN pipeline (11), which automatically reconstructs multiple sequence alignments and phylogenies and that identifies events of gene duplication, recombination as well as marks of positive selection based on a coding sequence (Fig. 1*D*). Automated or manually retrieved sequences of primary hits were used as query for DGINN. We performed analyses in two steps: 1) phylogenetic analyses, and 2) positive selection analyses that combine five methods from PAML Codeml, HYPHY BUSTED, and bpp packages (see *Materials and Methods*). We found five genes with evidence of strong positive selection in primates, detected by at least four methods (Fig. 1*D* and *SI Appendix*, Fig. S2 *A–C*): absent in melanoma 2 (AIM2), the leukocyte immunoglobulin like receptor LILRA3, the CASP8- and FADD-like apoptosis regulator (CFLAR), the 6-methylated adenosine (m6A) reader IGF2BP3, and Trim69, a poorly studied member of the TRIM family. Five additional genes exhibited some evidence of positive selection, detected by two to three methods: the bromodomain adjacent to zinc finger domain 1A (BAZ1A), the DNA topoisomerase I (TOP1), the A-kinase anchoring protein 2 (AKAP2), the proteasome subunit beta type-8 (PSMB8), and transportin 3 (TNPO3) (Fig. 1*D*).

Trim69 Is a Novel Broad Inhibitor of Viral Infection. Among the top hits, we focused on Trim69, a prototypical member of the C-IV subfamily of Trims (14), which includes Trim5α which is a well-established antiviral factor against primate lentiviruses. Trim69 possesses a RING, B-box, and coiled-coil (CC) domain followed by a PRY-SPRY domain. Trim69 bears 48% and 44% identity with Trim67 and Trim52/Trim47 following a Blast analysis, while its SPRY domain is closer to Trim39 and Trim21 (46% and 45% identity, respectively, *SI Appendix*, Fig. S3*A*). Comparison between the in silico modeled SPRY domains of Trim69 and Trim5α indicates that Trim69 lacks the protruding variable loops (V1, V2, and V3) with which Trim5α contacts specifically retroviral capsids, suggesting an altogether different method of action (*SI Appendix*, Fig. S3*B*).

Despite having being first identified as a spermatids-specific gene (4), Trim69 exhibits a heterogeneous pattern of expression in different cell lines and primary blood cell types tested (*SI Appendix*, Fig. S4*A*). In THP-1-PMA cells, Trim69 is expressed already at basal levels and is extremely sensitive to IFN-I (α/β) stimulation, similarly to primary macrophages. To first validate the results obtained in our screen, we generated Trim69 knockout (KO) THP-1 cells by CRISPR-/Cas9-mediated gene deletion (*SI Appendix*, Fig. S4*B* for cell viability) and then challenged macrophage-differentiated cells with HIV-1, HIV-2, or SIV_{MAC} lentiviruses in the presence or absence of IFN-α. Under these conditions, removal of Trim69 increased the susceptibility of target cells to the three primate lentiviruses in the presence, but also in the absence of IFN-α (from 2.25 to 3.35 on average), in line with its expression pattern (Fig. 1*E*). Conversely, and as expected for an antiviral factor, the susceptibility of THP-1 PMA cells stably expressing TRIM69 under the control of doxycycline (overexpressing [OE]; *SI Appendix*, Fig. S4*B* for cell viability) was decreased to the same extent during infection with these retroviruses (Fig. 1*F*). Given that in this set of experiments viruses were pseudotyped with the pantropic envelope VSVg, Trim69 KO and OE cells were also challenged with an HIV-1 virus bearing the R5-tropic HIV-1 envelope JR-FL and similar results were obtained, indicating that the antiviral effects of Trim69 were envelope-independent (Fig. 1*G*).

In agreement with two previous reports (9, 10), Trim69 also potently modulated replication of the negative-strand RNA virus, VSV (Fig. 1*H*). Next, we examined the ability of Trim69 to interfere with the replication of SARS-CoV-2, a positive-strand RNA coronavirus, in epithelial lung Calu-3 cells. Under these conditions, Calu3 expressing Trim69 were strongly protected from SARS-CoV-2 infection (Fig. 1*I*), overall indicating that Trim69 is able to interfere with a broad range of RNA viruses that extends from retroviruses to positive- and negative-strand RNA viruses (*SI Appendix*, Fig. S5 for non-normalized values of infection with the different viruses). Given that SARS-CoV-2 entry in Calu3 cells can occur at both plasma membrane and endo-lysosomes (15), we used Camostat to inhibit TMPRSS2 and to skew virus entry via the latter entry route. Albeit with lower efficiency, Trim69 remained able to inhibit SARS-CoV-2 infection, further strengthening the contention that the virus entry pathway is not a major determinant of susceptibility to Trim69 (*SI Appendix*, Fig. S6*A*). Of note, Trim69 overexpression did not inhibit lentivirus infection in HEK293T cells, in agreement with one previous report (9). Inhibition of VSV replication occurred in these cells, albeit to a lower magnitude with respect to what observed in the case of THP-1-PMA cells (*SI Appendix*, Fig. S6*B*), suggesting that the extent of the effects of Trim69 may be governed by a combination of both virus and cell-type-specific features.

Trim69 Inhibits HIV-1 Reverse Transcription and the Early Phases of VSV and SARS-CoV-2 Infection. To identify the step(s) at which Trim69 interfered with virus replication, Trim69-overexpressing THP-1-PMA or Calu3 cells were challenged with the different viruses and the early phases specific to each one were analyzed (schematically resumed in Fig. 2 *A–C*). In the case of Lentiviruses, THP-1-PMA OE cells were challenged with R5-HIV-1, and virus entry into the cell was measured using the EURT assay [entry/uncoating assay based on core-packaged RNA availability and Translation (16)], which is based on the direct translation of a Luciferase-bearing HIV-1 minigenome incorporated into virion particles (Fig. 2*A*). Under these conditions, Trim69 did not affect HIV-1 entry. On the

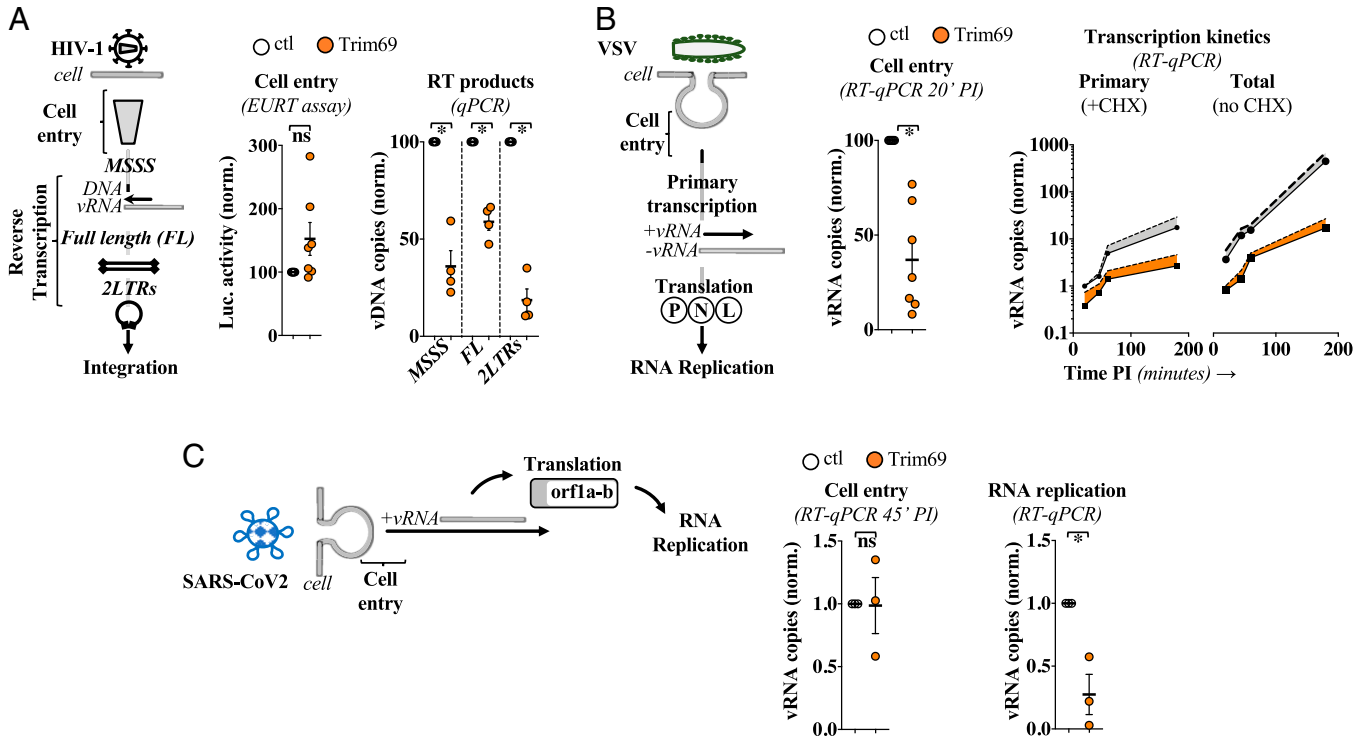

Fig. 2. Trim69 inhibits the initial steps of infection of different viruses. (*A*) As schematically presented, virus entry and accumulation of reverse transcription DNA intermediates were measured in THP-1-PMA cells overexpressing or not Trim69 upon challenge with an R5-tropic Env HIV-1. Cell entry was tested according to the EURT assay, an HIV-1-based cell entry assay based on the direct translation of an HIV genome carrying the Firefly luciferase. To ensure complete exposure of viral RNA, infections were carried out in the presence of 10 μM of PF74. (*B*) VSV cell entry and RNA transcription steps were similarly tested in THP-1-PMA cells. Cell entry was quantified by measuring the levels of viral RNA that entered cells 20 min after viral challenge and trypsin treatment of target cells to remove unbound virus. Pioneer and whole RNA replication were discriminated by performing infections at an MOI of 1 in the presence or absence of 100 μg/mL of CHX. (*C*) As in (*B*) for SARS-CoV-2. The extent of infection was determined in Calu3 cells ± Trim69 at 45-min post-infection and after a trypsin treatment to remove non-internalized viruses. Viral RNA replication was then determined by RT-qPCR at 6-h post-infection to focus on early events. Graphs present average and SEM of three to seven individual experiments. ns, non-significant. *$P < 0.05$ following a two-tailed Student's *t* test between the indicated conditions.

contrary, Trim69 impaired the accumulation of all HIV-1 viral DNA intermediates tested (2.7-fold for MSSS to 5.3-fold for 2LTRs), indicating that this protein inhibits reverse transcription rapidly after the entry of viral capsids in target cells.

VSV is a negative-strand RNA virus and, as such, it undergoes an obligate round of primary transcription after cell entry that is required for the translation of P, N, and L proteins that in turn ignite viral RNA replication [for a review see (17), Fig. 2*B*]. Given that translation from primary transcripts is required for viral RNA replication, the translation inhibitor cycloheximide (CHX) can be used to distinguish primary transcription from overall RNA replication. Contrarily to what was observed for HIV-1, TRIM69 exerted a measurable defect in VSV entry into the cell (2.9-fold), and this defect increased during primary transcription (6.5-fold) and overall RNA replication levels (34-fold). Thus, in the case of VSV, Trim69 imparts successive cumulative antiviral effects.

SARS-CoV-2 is a positive-strand RNA virus and, as such, its genome can be directly translated in viral proteins that ignite RNA replication [for a review see (18)].

When Calu-3 cells overexpressing Trim69 were challenged with SARS-CoV-2, no major defects were observed at entry, but a defect in RNA replication was clearly observable by 6 h post-infection (Fig. 2*C*, 3.6-fold, in line with the replication defect observed).

Overall, these results indicate that Trim69 inhibits the early steps of viral replication of different viruses at slightly distinct steps: at a post entry step that affects the efficiency of reverse transcription and of viral RNA replication in the case of lentiviruses and of the SARS-CoV-2 coronavirus, and at both entry and post entry events in the case of VSV. In the latter, the efficiency of virus entry in cells expressing Trim69 exhibits a small but detectable defect, together with a more apparent defect in primary transcription.

Trim69 Is a Novel Regulator of Stable Microtubule Dynamics. As a first step to decorticate the functions of Trim69, its intracellular distribution was determined by confocal microscopy. In agreement with a previous report (10), Trim69 adopts a filamentous distribution in the cell cytoplasm which is particularly marked in THP-1-PMA cells (Fig. 3*A*). Exploratory analyses indicated that Trim69 exhibited little to no colocalization with a series of cellular markers in HEK293T cells (actin, ATG-3, ER, or CLIP170), with the exception of α-tubulin (*SI Appendix*, Fig. S7). Indeed, Trim69 colocalized strongly in all cell tested with stable microtubules (defined here upon staining with either anti-acetylated or anti-detyrosinated tubulin-specific antibodies) which represent a subset of MTs (Fig. 3*B*). Interestingly, Trim69-expressing cells exhibited higher levels of stable microtubules, suggesting that this protein could promote their formation.

To put this observation in the context of IFN-I responses, we determined whether microtubule stabilization could be observed in response to IFN-I in different primary blood cells (Fig. 3*C* and *SI Appendix*, Fig. S8 for separated channels and quantification of stable MTs on a per cell basis). Stimulation of primary blood monocytes as well as of monocyte-derived macrophages and dendritic cells (DCs) led to a pronounced up-regulation of stable microtubules within 24–48 h (monocytes > macrophages > DCs). In contrast, such accumulation was not observed in activated primary lymphocytes. Overall, these results indicate

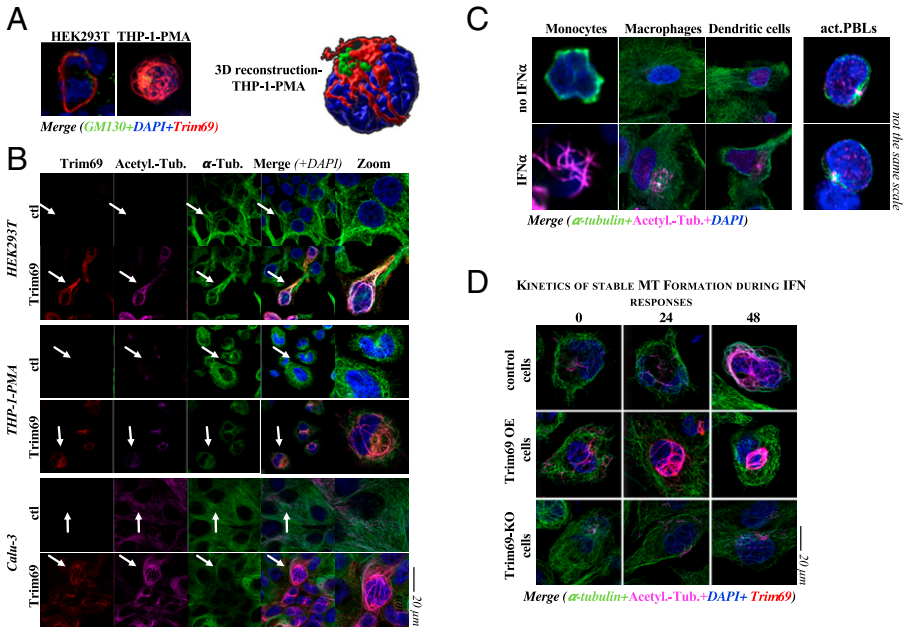

Fig. 3. Trim69 is a key mediator of IFN-I induced microtubule stabilization. (*A*) Representative confocal microscopy pictures and 3D reconstruction of the intracellular distribution of Trim69 in HEK293T and THP-1-PMA cells. (*B*) Distribution of Trim69 with antibodies recognizing endogenous α-tubulin or its acetylated form in the indicated cell types. Arrows indicates the cell zoomed on the *Right* panels. (*C*) Primary blood monocytes, macrophages, dendritic cells (DCs), as well as PH1/IL2-activated PBLs were stimulated or not with 1.000 U/mL of IFN-α for 24 and 48 h prior to fixation and confocal microscopy analysis. Representative cells at 24 or 48 h are presented here, while the quantification of stable microtubules, at all the time points are presented in the *SI Appendix*, Fig. S8. Given the large differences in cell size, the pictures do not use the same scale. (*D*) As in (*B*) in THP-1-PMA cells either control (*wild-type*) or in which Trim69 was either OE or KO, respectively. Pictures present typical results obtained in greater than three independent experiments in over 50 cells examined per condition. Separated channels for the images in (*C*) and (*D*), in addition to the quantification of the amounts of stable MTs, are provided in the *SI Appendix*, Figs. S8 and S9.

that IFN leads to a program of microtubule stabilization that may be particularly important for antiviral responses in cells of myeloid origins.

To determine the role that Trim69 may play in this program, we used THP-1 (cells of myeloid origins more amenable to genetic manipulation). In control cells, stable MTs were present at low levels in the absence of IFN stimulation, but they increased over time following IFN-α stimulation similarly to what was observed in primary macrophages (Fig. 3*D* and *SI Appendix*, Fig. S9 for complete pictures and quantification of stable MTs on a per-cell basis). As expected from our previous observations, expression of Trim69 (OE) increased the basal levels of stable microtubules accumulation and this was further stimulated by IFN-α. However, the accumulation of stable microtubules was severely diminished in Trim69 KO cells stimulated with IFN-α, indicating that the accumulation of stable microtubules is an integral part of the antiviral IFN response and that Trim69 plays an instrumental role in this program.

Taxol is a compound that also leads to the accumulation of stable MTs in cells. To determine whether the program of MTs stabilization induced by Trim69 was specific or similar to the one induced by Taxol, control or Trim69 overexpressing THP-1-PMA cells were incubated for 24 h with either Taxol or nocodazole (that instead depolymerizes MTs), and then cells were either analyzed by confocal microscopy or challenged with VSV prior to flow cytometry (*SI Appendix*, Fig. S10). Under these conditions, Taxol exerted a slightly positive effect on VSV infectivity in control cells, while nocodazole led to a specular decrease, in line with previous reports (19, 20). However, neither Taxol nor nocodazole modified the extent of virus inhibition driven by Trim69, strongly supporting the notion that Trim69 drives a specific program of MTs stabilization that is distinct from the one induced by Taxol. Of interest, confocal microscopy analysis revealed differences in the arrangement of stable microtubules that accumulate in the presence of Taxol or Trim69 (*SI Appendix*, Fig. S10, compare the arrangement of stable microtubules in the zoomed control cell treated with Taxol or in the Trim69 overexpressing one), further corroborating the notion of specificity in the action of Trim69.

Trim69 Directly Associates to Microtubules. To determine whether Trim69 could physically associate to microtubules, a microtubule polymerization/sedimentation assay (21) was performed on THP-1 cell lysates expressing or not expressing Trim69. In this assay, tubulin is induced into polymerization upon incubation with GTP and Taxol, and stabilized microtubules are then purified by ultracentrifugation, along with associated cellular proteins (scheme of Fig. 4*A*). Accordingly, a large fraction of microtubules sedimented in the pellet fraction upon Taxol stabilization and, when present, Trim69 was also present in this fraction, indicating that Trim69 was indeed physically associated to microtubules (Fig. 4*A*, fraction P). To determine whether this association was direct, Trim69 was purified from bacteria as a fusion protein with the glutathione-S-transferase protein (GST). Commercially available and pure tubulin was then incubated in the presence of GTP and Taxol before binding to either GST or GST-Trim69 (Fig. 4*B*). Under these conditions, Trim69 was able to interact with microtubules, indicating that the association between these two components is direct and not bridged by other factors.

Stable Microtubule Formation Is Key to the Antiviral Effects of Trim69. Five different isoforms issued from alternative splicing have been recently described for *trim69* (from the *wild-type* A to E) that contain extensive deletion in domains that are normally important for Trim family member's functions. These isoforms were therefore expressed in THP-1-PMA cells prior to confocal microscopy analysis, or viral challenge with VSV

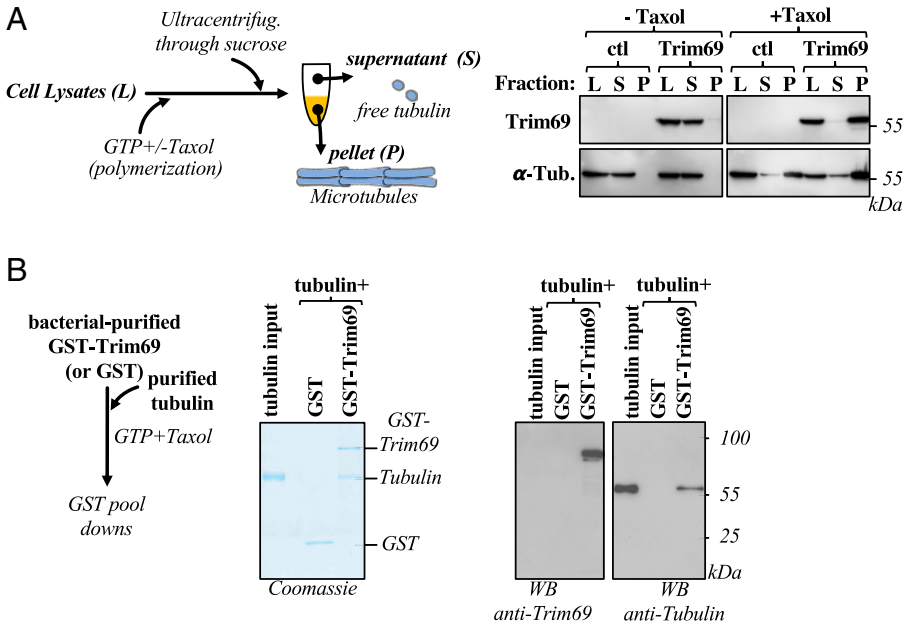

Fig. 4. Trim69 associates directly to microtubules. (*A*) Schematic representation of the microtubule sedimentation assay used. Briefly, the cytosolic fraction of THP-1-PMA cells expressing or not Trim69 was harvested, and free cellular tubulin polymerization and stabilization was induced by incubation with GTP and Taxol. Microtubules and associated cellular proteins were then purified through a sucrose gradient prior to WB analysis. (*B*) Direct binding between tubulin and Trim69 was assessed by using commercially available pure tubulin and GST-Trim69 purified from bacteria. The Coomassie and WB panels are representative of three independent experiments.

(Fig. 5 *A* and *B* and *SI Appendix*, Fig. S11 for Western blot [WB] analysis and separated immunofluorescence (IF) channels). Under these conditions, isoforms B to E lost their ability to stimulate stable MTs and to protect target cells from viral challenge. Two additional mutations were then introduced in Trim69: mutations in two cysteine residues in the RING domain (C61A/C64A), in addition to the deletion of the PRY-SPRY domain that in certain Trim members represents the domain of interaction with cellular partners (ΔP-SPRY, Fig. 5 *A* and *B* and *SI Appendix*, Fig. S11, as above). Similarly, to what was observed with the Trim69 isoforms, both mutants lost their ability to drive stable MT accumulation and both were unable to prevent viral infection. To gather further insights on the ability of the different mutants not only to stimulate stable microtubules, but also to colocalize with α-tubulin, the Pearson's coefficients between these two markers were determined (Fig. 5*A*). Colocalization with α-tubulin was lost for all mutants, suggesting that they have likely lost their ability to associate to microtubules in the first place. Similar results were also obtained in HEK293T cells that do not express Trim69 (*SI Appendix*, Fig. S12), thus excluding the possibility that the expression of endogenous Trim69 in THP-1 cells interfered with the analysis of the intracellular distribution and behavior of Trim69 mutants through heterodimerization. To assess the ability of Trim69 mutants to directly bind MTs also in vitro, we employed GST-pulldowns and compared the ability of wild-type (WT), C61A/C64A, and ΔP-SPRY Trim69-GST proteins to associate to pure microtubules. Under these conditions, a drastic loss of association was observed for the C61A/C64A mutant in agreement with the loss of MTs association observed by confocal microscopy (*SI Appendix*, Fig. S13*A*). However, the ΔP-SPRY Trim69 mutant remained able to associate to MTs, albeit with lower efficiency with respect to WT, somewhat unexpectedly given the distribution of this mutant in the cell. One plausible explanation for this difference could be that association of Trim69 to MTs is more stringent in cells than in vitro (differences in the relative concentration of the two components in the two systems, need to displace MT-bound factors, etc.). Finally, we tested the ability of the two above-mentioned Trim69 mutants to undergo self-ubiquitination, which is often used to measure the weight of the E3-ubiquitin ligase activity in Trim functions (22). To this end, cells were cotransfected with DNAs coding WT, C61A/C64A, and ΔP-SPRY Trim69 along with HA-ubiquitin in the presence of MG132, prior to cell lysis, immunoprecipitation of Trim69 and WB analysis (*SI Appendix*, Fig. S13*B*). Under these conditions, WT Trim69 was clearly ubiquitinated, similarly to the two mutants. While inactivation of the E3-ubiquitin ligase activity of Trim69 could have been expected upon inactivation of the two cysteines in position 61 and 64, it is important to remember that the RING domain is composed of seven cysteines and one histidine, the importance of which varies according to the Trim protein examined (22). Overall, these results would thus suggest that the E3-ubiquitin ligase activity of Trim69 is not important in the functions described here given that two loss of function mutants remain competent for their E3-ubiquitin ligase activity. However, given that the Trim69 cellular targets are unknown and that this assay measures only the ability of Trim69 to self-ubiquitinate, it remains possible that these mutants are inactive because they can no longer ubiquitinate their correct targets.

Overall, the major conclusion of these results is that that the antiviral effects of Trim69 are intimately linked to its ability to drive the accumulation of stable MTs.

Induction of Stable MTs, As Well As Antiviral Functions, Are Conserved in a Nonhuman Divergent Primate Trim69 Ortholog. To increase the primate sequences available for phylogenetic analyses (7, 9), we de novo sequenced Trim69 from two additional monkey species, L'Hoest's monkey (*Cercopithecus l'hoesti*) and Cotton-headed tamarin (*Saguinus oedipus*) (Fig. 6*A*), and we determined the evolutionary history of Trim69 inferred from 26 primate species and 22 simian species (Fig. 6 *A* and *B* and *SI Appendix*, Fig. S14). From these codon alignments, we used multiple methods to detect positive selection at the gene-

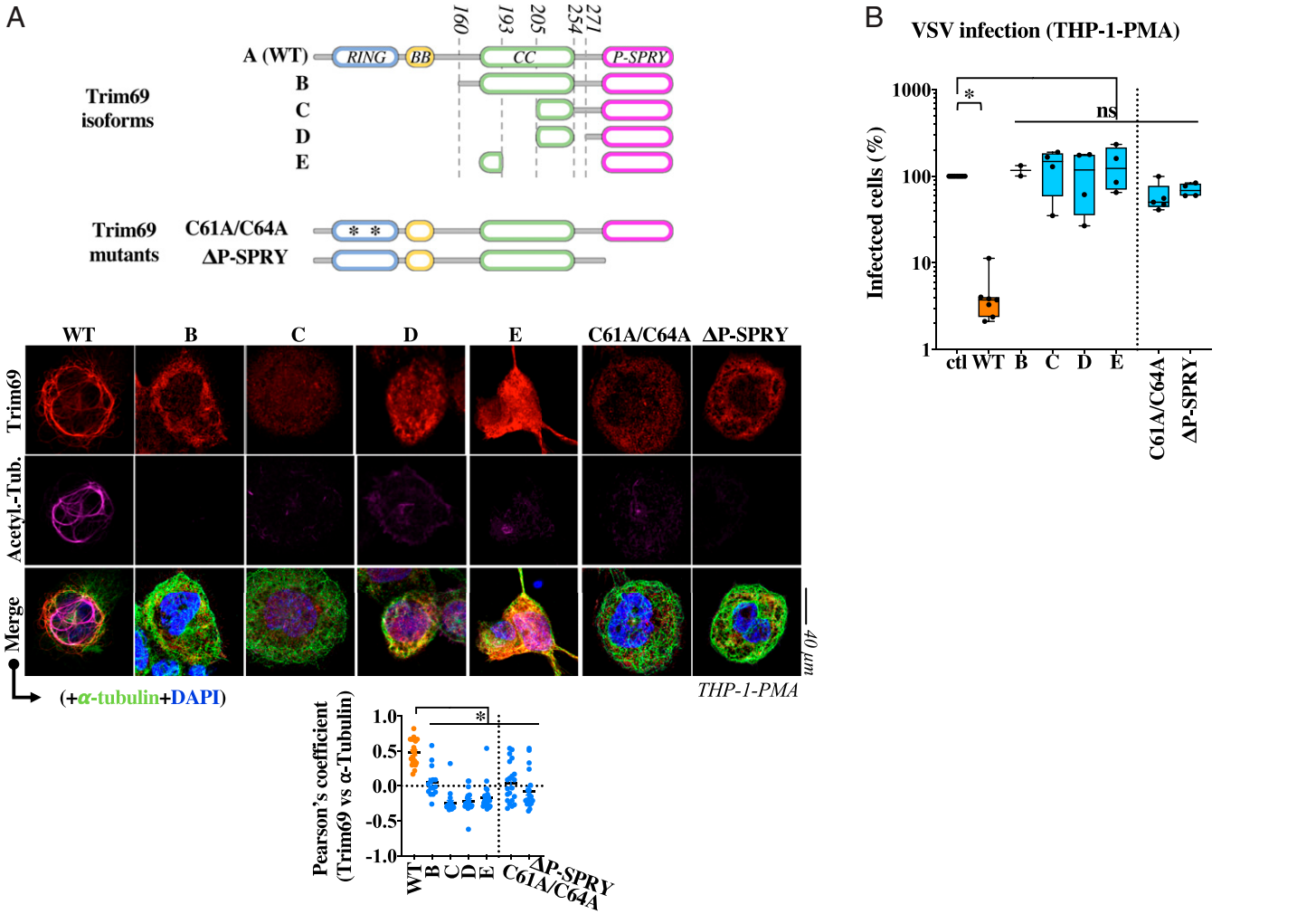

Fig. 5. The ability of Trim69 to stimulate stable MTs is intimately linked to its antiviral abilities. (*A*) Schematic presentation of Trim69 domains, isoforms, and mutants used here. Mutants were evaluated for their ability to stimulate stable MTs formation in THP-PMA cells by confocal microscopy. The graph presents Pearson's coefficients calculated between Trim69 mutants and α-tubulin in 24–15 cells. *Statistical significant differences between each mutant and WT, following an ordinary one-way ANOVA with Dunnett's multiple comparison test. Representative WB panels of the different mutants in THP-1-PMA cells are provided in the *SI Appendix*, Fig. S10. (*B*) Cells were also challenged with an MOI of 0.1 of VSV, prior to flow cytometry analysis 18 h later. Pictures display representative patterns obtained and the box and whiskers presents data obtained from two to four independent experiments. ns, non-significant. *$P = 0.0005$ following an ordinary one-way ANOVA with Dunnett's multiple comparison test of the indicated samples over control.

wide and site-specific levels: BUSTED from HYPHY, Codeml from PAML and Bio++ analyses, all run from the DGINN platform, as well as MEME and FUBAR run from the Datamonkey server (see *Materials and Methods* for details and references). We confirmed that Trim69 has been under adaptive evolution (*SI Appendix*, Fig. S14). The site-by-site analyses on the simian alignment allowed us to identify eight sites under positive selection distributed through the protein domains, with three residues (158, 246, and 299) identified by at least two methods (Fig. 6 *B* and *C* and *SI Appendix*, Fig. S14). Because the soTrim69 was one of the most divergent simian sequences from hTrim69 (88.6% identity; Fig. 6*B*) and differed at seven of eight sites under positive selection, we cloned the soTrim69 gene to determine whether it exhibited distinct, or conserved, functionalities compared to its human counterpart. Stable THP-1-PMA cells expressing each of them were challenged with the indicated viruses prior to analysis by WB, confocal microscopy, and flow cytometry to quantify the extent of infection (Fig. 6*D*). Under these conditions, soTrim69 was capable of strong induction of stable microtubule formation and exhibited equivalent antiviral properties than hTrim69 upon challenge with VSV or distinct lentiviruses. Overall, these results indicate that the main functional properties are maintained in the soTrim69 ortholog underscoring their importance in the antiviral properties of Trim69. Our data also indicate that lentiviruses are unlikely to have driven positive selection in Trim69.

Discussion

In this work, we describe Trim69 as the IFN-regulated protein that inhibits a diverse spectrum of viruses by promoting a global program of microtubule stabilization in the cell that is markedly distinct from the one induced by Taxol. By analyzing the response of several primary blood cell types to IFN-α, we show that this program is a previously unrecognized facet of the innate defense system in cells of the myeloid lineage. Furthermore, using THP-1 cells that are more amenable to genetic manipulation, we show that Trim69 plays an instrumental role in this response. Trim69 interferes with model members of the *Retroviridae*, *Rhabdoviridae*, and *Coronaviridae* families that collectively cover a large representation of replication modes among RNA viruses. The magnitude of inhibition depends on the combination between virus and cell type and in the cases of Lentiviruses, the antiviral effect is observed essentially in

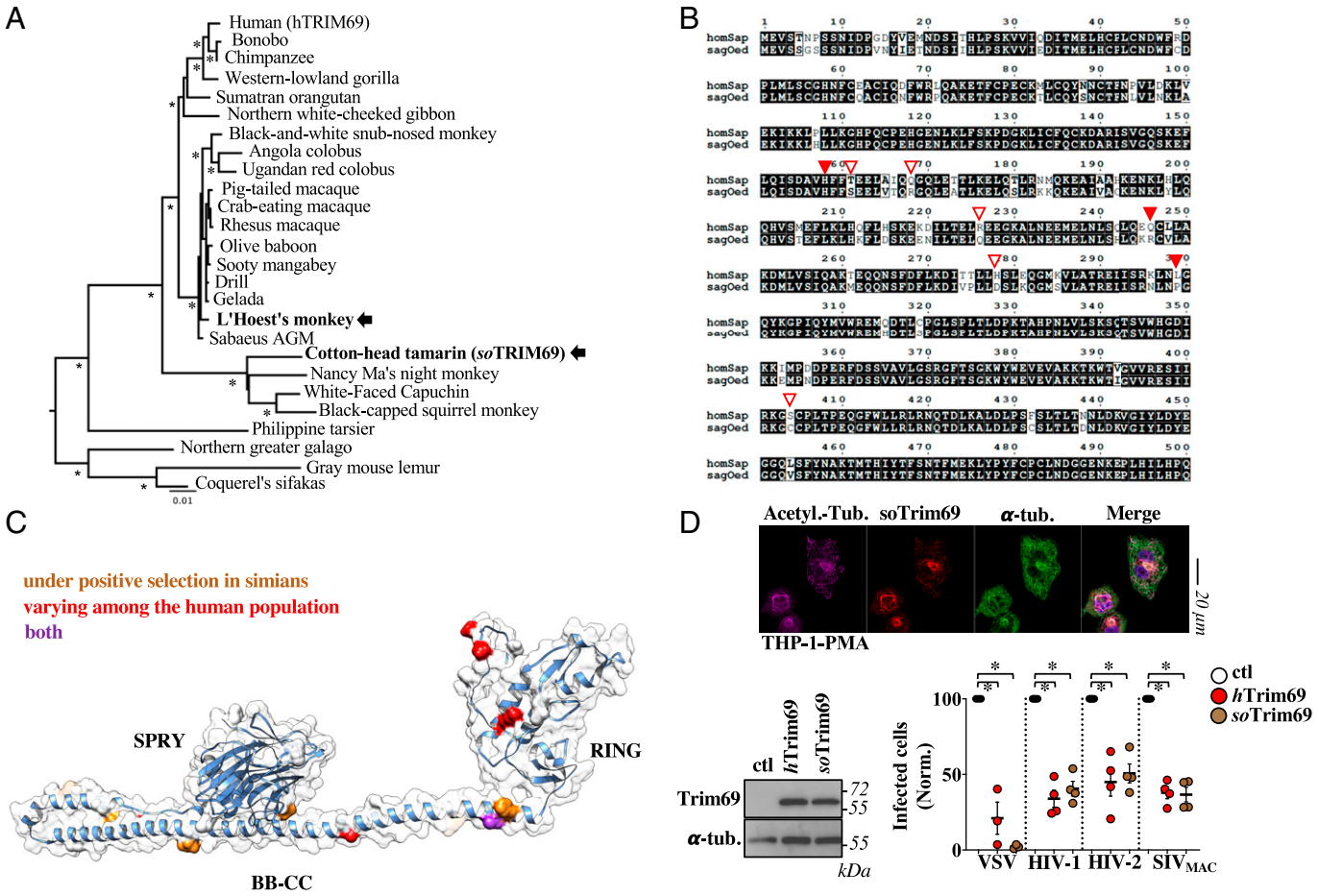

Fig. 6. Trim69 exhibits signatures of positive selection during primate evolution and the divergent Trim69 ortholog from *Saguinus oedipus* (soTrim69) also inhibits viral infection and drives microtubule changes. (*A*) Phylogenetic tree of primate Trim69, including two newly sequenced orthologs from L'Hoest's monkey and Cotton-head tamarin (arrows). PhyML was run with GTR+I+G model and 1,000 bootstrap replicates for node statistical supports (asterisks represent values above 700/1000). Sequence references are shown in *SI Appendix*, Fig. S11*A*. (*B*) Amino acid alignment of human and cotton-headed tamarin Trim69 (88.6% identity). Representation with ESPript (43). Sites under positive selection are highlighted with red triangles (plain triangles, sites identified by greater than two methods; open triangles, sites identified by one method). (*C*) Amino acid positions undergoing positive selection or allelic variations in the human population are presented in the modeled 3D structure of human Trim69. (*D*) Functional equivalency of the soTrim69 ortholog with respect to the induction of stable microtubule formation and to antiviral activities against VSV ($n = 3$) and primate lentiviruses ($n = 4$). Experiments present average and SEM. *$P < 0.05$ following a two-tailed Student's t test between Trim69 proteins and respective controls.

cells of the myeloid lineage. This is not unprecedented as other cellular factors inhibit HIV-1 in a cell-type-specific manner [e.g., SAMHD1, or APOBEC3A (23, 24)].

Viral inhibition occurs during the early phases of the different viruses' life cycle, albeit with slight differences. In the case of HIV-1, inhibition occurs at reverse transcription after entry of viral complexes into the cell, and SARS-CoV-2 seems to follow the same inhibitory path, with no measurable defects in virus entry but an early defect in viral RNA replication. Instead, a small but non-negligible defect can be observed at the step of entry in the case of VSV, which is then followed by an additional defect during pioneer transcription, in line with a previous report (10).

Although it remains formally possible that Trim69 targets viral components, the very diversity of viruses examined here lends support to the hypothesis that Trim69 modifies the cellular environment in a manner that is preclusive to viral infection. The hypothesis we privilege is that Trim69 interferes with the movements of viral complexes along microtubules. Indeed, HIV-1 viral cores have been visualized as sliding along microtubules with inward rates of 1 μm/s consistent with Dynein-dependent movement (20, 25), and adaptor proteins of this complex have been involved in this association [e.g., the Bicaudal D2 adaptor, BICD2 (26)]. Interestingly, interference with dynein-dependent movement has been associated to an early reverse transcription defect (27) which is consistent with the defects observed here for Trim69 (27). In the case of Rhabdoviruses, the phosphoprotein P, which is part of the viral nucleoprotein complex along with the nucleocapsid protein (N) and the RNA polymerase (L), does interact with the dynein light chain 8 (LC8) (28) and Coronaviruses accumulation in the perinuclear region that evolves in double membrane vesicles (DMVs) is also influenced by dynein (29). It is thus possible that dynein transport is inhibited in the presence of stable microtubules that are decorated with Trim69.

Several viruses have been described to induce stable MTs formation: herpesviruses (30, 31), influenza virus (32), hepatitis E virus (33), and adenovirus (34, 35) as well as HIV-1 (36–38). While in some studies the functional importance of stable MT formation remains unclear, and according to our data could even represent a cellular response to viral infection, there are cases in which MT stabilization is associated to a pro-viral functionality. This seems to be the case for HIV-1 in which viral capsids that enter target cells induce prompt MT stabilization and mimic cellular cap-loading proteins to promote their loading onto MTs and their dynein-dependent transport toward the nucleus (36–38).

It is therefore counterintuitive that IFN may induce a program of MT stabilization via Trim69, as this particular pool of MTs exhibit higher stability and higher cargo trafficking propensity with respect to the dynamic pool of MTs (39, 40).

We believe that this dichotomy is, however, only apparent. First, while it is true that stable MTs can be preferentially used for cargo transport, the initial step of cargo loading is instead highly inefficient when it occurs on microtubules that are already detyrosinated (i.e., stable) (41). As such, it is easy to envision that according to the timing at which microtubules become stabilized with respect to virus entry, MT stabilization can lead to either pro- or anti-viral outcomes.

Second, while stable MTs are often considered as a single homogeneous entity, the existence of several posttranslational modifications on MTs, as well as the existence of numerous MT-bound factors, is likely to result in a far more complex functional heterogeneity of microtubules. In line with this contention, our study indicates that as part of an antiviral response, Trim69 starts a program of microtubule stabilization that lead to structures whose functionality is markedly antiviral, while Taxol that also leads to the accumulation of stable MTs exerts slight positive effects on viral infection.

Trim69 binds directly to MTs, but contrarily to other members of the Trim family, we could not identify a C-terminal subgroup one signature (COS domain), a 60-amino acid stretch that mediates MT binding in certain Trim family members (42). We then show that intact RING and PRY-SPRY domains are required for the antiviral activities of Trim69, as well as for microtubule stabilization. In light of these results, a most plausible model would therefore be that Trim69 associates to microtubules and contacts relevant substrates via its PRY-SPRY domain, leading to their degradation. However, the importance of the E3-ubiquitin ligase activity in the functions of Trim69 is debated, and the RING domain has also been shown to promote the protein's multimerization (8, 10). In our hands, the loss-of-function mutants examined here are able to undergo self-ubiquitination, suggesting that the E3-ubiquitin ligase activity of Trim69 may not be involved in the phenotypes described here. We would, however, caution about a quick dismissal of the importance of this property because it remains formally possible that Trim69 mutants have lost their phenotype and because they can no longer target their correct cellular targets, a likely possibility with protein mutants that exhibit drastic changes in localization in the cell, when compared to *wild-type*. As such, we believe that the relevance of the E3-ubiquitin ligase activity of Trim69 in the phenotypes described here remains still open.

Finally, three studies, including the present one, have accumulated evidence of ongoing genetic conflict in primate Trim69 (7, 9), as well as of polymorphism in the human population. Using a very divergent simian Trim69, our results seem to exclude Lentiviruses that have invaded primates as main drivers of this selective pressure. However, Trim69 has been described to physically interact with the P protein of VSV and with the NS3 protein of Dengue virus (8–10), suggesting that viral antagonists of these or of other viral families that remain to be discovered may have exerted a genetic pressure on Trim69.

Overall, in a panorama filled with positive cofactors at the level of cytoskeleton, Trim69 represents for the moment the antiviral factor that opposes viral infection by regulating microtubule dynamics. Given the fact that these structures influence several aspects of the cellular physiology, these findings may bear implications that extend beyond viral infection.

Materials and Methods

Trim69 was identified as relevant hit following an shRNA-based genetic screen that examined the weight of 419 ISGs during HIV-1 infection in macrophage-like THP-1-PMA cells stimulated with interferon. Using stable cells overexpressing or knocked out for Trim69, we have demonstrated that Trim69 acted as broad antiviral factor. Using confocal microscopy and in vitro binding assays, we have then determined that Trim69 binds MTs and it drives a program of MT stabilization in cells required for its antiviral activities. Detailed methods are in *SI Appendix*.

Data, Materials, and Software Availability. Source data and reagents are available with no restriction. All study data are included in the article and/or *SI Appendix*.

ACKNOWLEDGMENTS. We thank Laurent Guéguen (LBBE-Lyon) for fruitful discussions on phylogenetic analyses, Didier Négre and Philippe Mangeot (CIRI-Lyon), and Pei-Yong Shi (University of Texas Medical Branch, Galveston, TX) for sharing of material, the authors that provided material through Addgene, and the contributors of publicly available genomic and genetic sequences, as well as of phylogenetic programs. We thank Branka Horvat (CIRI, Lyon) for sharing B95a cells, as well as Guillaume Douay and the Zoo de Lyon for their collaboration. We acknowledge the contribution of the microscopy (LYMIC-PLATIM) platform of SFR BioSciences Gerland Lyon Sud (UMS3444/US8). Y.S. is the recipients of a PhD fellowship from the Chinese Scholarship Council. A.K. and C.d.S. have been recipients of a post-doctoral fellowship from the ANRS|MIE. This work has been supported by grants from the ANRS (AO-2014-1 and AO-2021-1 to A.C. and ECTZ19143 and ECTZ118944 to L.E.) and the ANR LABEX ECOFECT (ANR-11-LABX-0048 Investissements d'Avenir [ANR-11-IDEX-0007] of the UdL to L.E.). A.C. and L.E. are researchers of the Centre National de la Recherche Scientifique (CNRS). The funders had no role in study design, data collection and analysis, decision to publish, or preparation of the manuscript.

Author affiliations: [a]Centre International de Recherche en Infectiologie, Université de Lyon, Inserm, U1111, Université Claude Bernard Lyon 1, CNRS, UMR5308, École Nationale Supérieure de Lyon, Lyon, France

1. S. Cordeil *et al.*, Evidence for a different susceptibility of primate lentiviruses to type I interferons. *J. Virol.* **87**, 2587–2596 (2013).
2. R. Rajsbaum, A. García-Sastre, G. A. Versteeg, TRIMmunity: The roles of the TRIM E3-ubiquitin ligase family in innate antiviral immunity. *J. Mol. Biol.* **426**, 1265–1284 (2014).
3. R. Sinnott *et al.*, Mechanisms promoting escape from mitotic stress-induced tumor cell death. *Cancer Res.* **74**, 3857–3869 (2014).
4. H. W. Shyu, S. H. Hsu, H. M. Hsieh-Li, H. Li, A novel member of the RBCC family, Trif, expressed specifically in the spermatids of mouse testis. *Mech. Dev.* **108**, 213–216 (2001).
5. H. W. Shyu, S. H. Hsu, H. M. Hsieh-Li, H. Li, Forced expression of RNF36 induces cell apoptosis. *Exp. Cell Res.* **287**, 301–313 (2003).
6. X. Rong *et al.*, TRIM69 inhibits cataractogenesis by negatively regulating p53. *Redox Biol.* **22**, 101157 (2019).
7. R. Malfavon-Borja, S. L. Sawyer, L. I. Wu, M. Emerman, H. S. Malik, An evolutionary screen highlights canonical and noncanonical candidate antiviral genes within the primate TRIM gene family. *Genome Biol. Evol.* **5**, 2141–2154 (2013).
8. K. Wang *et al.*, Interferon-stimulated TRIM69 interrupts dengue virus replication by ubiquitinating viral nonstructural protein 3. *PLoS Pathog.* **14**, e1007287 (2018).
9. S. J. Rihn *et al.*, TRIM69 inhibits vesicular stomatitis Indiana virus. *J. Virol.* **93**, e00951-19 (2019).
10. T. Kueck *et al.*, Vesicular stomatitis virus transcription is inhibited by TRIM69 in the interferon-induced antiviral state. *J. Virol.* **93**, e01372-19 (2019).
11. L. Picard *et al.*, DGINN, an automated and highly-flexible pipeline for the detection of genetic innovations on protein-coding genes. *Nucleic Acids Res.* **48**, e103 (2020).
12. A. L. Brass *et al.*, Identification of host proteins required for HIV infection through a functional genomic screen. *Science* **319**, 921–926 (2008).
13. M. D. Daugherty, H. S. Malik, Rules of engagement: Molecular insights from host-virus arms races. *Annu. Rev. Genet.* **46**, 677–700 (2012).
14. W. Yang, Z. Gu, H. Zhang, H. Hu, To TRIM the immunity: From innate to adaptive immunity. *Front. Immunol.* **11**, 02157 (2020).
15. J. Koch *et al.*, TMPRSS2 expression dictates the entry route used by SARS-CoV-2 to infect host cells. *EMBO J.* **40**, e107821 (2021).
16. C. Da Silva Santos, K. Tartour, A. Cimarelli, A novel entry/uncoating assay reveals the presence of at least two species of viral capsids during synchronized HIV-1 infection. *PLoS Pathog.* **12**, e1005897 (2016).

17. R. G. Dietzgen, H. Kondo, M. M. Goodin, G. Kurath, N. Vasilakis, The family Rhabdoviridae: Mono- and bipartite negative-sense RNA viruses with diverse genome organization and common evolutionary origins. *Virus Res.* **227**, 158–170 (2017).
18. P. V'kovski, A. Kratzel, S. Steiner, H. Stalder, V. Thiel, Coronavirus biology and replication: Implications for SARS-CoV-2. *Nat. Rev. Microbiol.* **19**, 155–170 (2021).
19. M. H. Naghavi, Stable microtubule subsets facilitate early HIV-1 infection. *AIDS Res. Hum. Retroviruses* **30**, 211–212 (2014).
20. D. McDonald *et al.*, Visualization of the intracellular behavior of HIV in living cells. *J. Cell Biol.* **159**, 441–452 (2002).
21. S. Schweiger *et al.*, The Opitz syndrome gene product, MID1, associates with microtubules. *Proc. Natl. Acad. Sci. U.S.A.* **96**, 2794–2799 (1999).
22. C. Garcia-Barcena, N. Osinalde, J. Ramirez, U. Mayor, How to inactivate human ubiquitin E3 ligases by mutation. *Front. Cell Dev. Biol.* **8**, 39 (2020).
23. G. Berger *et al.*, APOBEC3A is a specific inhibitor of the early phases of HIV-1 infection in myeloid cells. *PLoS Pathog.* **7**, e1002221 (2011).
24. N. Laguette *et al.*, SAMHD1 is the dendritic- and myeloid-cell-specific HIV-1 restriction factor counteracted by Vpx. *Nature* **474**, 654–657 (2011).
25. N. Arhel *et al.*, Quantitative four-dimensional tracking of cytoplasmic and nuclear HIV-1 complexes. *Nat. Methods* **3**, 817–824 (2006).
26. A. Dharan *et al.*, Bicaudal D2 facilitates the cytoplasmic trafficking and nuclear import of HIV-1 genomes during infection. *Proc. Natl. Acad. Sci. U.S.A.* **114**, E10707–E10716 (2017).
27. P. Pawlica, L. Berthoux, Cytoplasmic dynein promotes HIV-1 uncoating. *Viruses* **6**, 4195–4211 (2014).
28. Y. Jacob, H. Badrane, P. E. Ceccaldi, N. Tordo, Cytoplasmic dynein LC8 interacts with lyssavirus phosphoprotein. *J. Virol.* **74**, 10217–10222 (2000).
29. W. Hou *et al.*, Dynamic dissection of dynein and kinesin-1 cooperatively mediated intercellular transport of porcine epidemic diarrhea coronavirus along microtubule using single virus tracking. *Virulence* **12**, 615–629 (2021).
30. G. Elliott, P. O'Hare, Herpes simplex virus type 1 tegument protein VP22 induces the stabilization and hyperacetylation of microtubules. *J. Virol.* **72**, 6448–6455 (1998).
31. A. R. Frampton, Jr *et al.*, Equine herpesvirus type 1 (EHV-1) utilizes microtubules, dynein, and ROCK1 to productively infect cells. *Vet. Microbiol.* **141**, 12–21 (2010).
32. M. Husain, K. S. Harrod, Enhanced acetylation of alpha-tubulin in influenza A virus infected epithelial cells. *FEBS Lett.* **585**, 128–132 (2011).
33. H. Kannan, S. Fan, D. Patel, I. Bossis, Y. J. Zhang, The hepatitis E virus open reading frame 3 product interacts with microtubules and interferes with their dynamics. *J. Virol.* **83**, 6375–6382 (2009).
34. J. C. Warren, L. Cassimeris, The contributions of microtubule stability and dynamic instability to adenovirus nuclear localization efficiency. *Cell Motil. Cytoskeleton* **64**, 675–689 (2007).
35. C. Yea, J. Dembowy, L. Pacione, M. Brown, Microtubule-mediated and microtubule-independent transport of adenovirus type 5 in HEK293 cells. *J. Virol.* **81**, 6899–6908 (2007).
36. S. Mitra, S. Shanmugapriya, E. Santos da Silva, M. H. Naghavi, HIV-1 exploits CLASP2 to induce microtubule stabilization and facilitate virus trafficking to the nucleus. *J. Virol.* **94**, e00404-20 (2020).
37. E. Santos da Silva *et al.*, HIV-1 capsids mimic a microtubule regulator to coordinate early stages of infection. *EMBO J.* **39**, e104870 (2020).
38. Y. Sabo *et al.*, HIV-1 induces the formation of stable microtubules to enhance early infection. *Cell Host Microbe* **14**, 535–546 (2013).
39. C. Janke, J. C. Bulinski, Post-translational regulation of the microtubule cytoskeleton: Mechanisms and functions. *Nat. Rev. Mol. Cell Biol.* **12**, 773–786 (2011).
40. R. Li, G. G. Gundersen, Beyond polymer polarity: How the cytoskeleton builds a polarized cell. *Nat. Rev. Mol. Cell Biol.* **9**, 860–873 (2008).
41. R. J. McKenney, W. Huynh, R. D. Vale, M. Sirajuddin, Tyrosination of α-tubulin controls the initiation of processive dynein-dynactin motility. *EMBO J.* **35**, 1175–1185 (2016).
42. K. M. Short, T. C. Cox, Subclassification of the RBCC/TRIM superfamily reveals a novel motif necessary for microtubule binding. *J. Biol. Chem.* **281**, 8970–8980 (2006).
43. X. Robert, P. Gouet, Deciphering key features in protein structures with the new ENDscript server. *Nucleic Acids Res.* **42**, W320–W324 (2014).